Liquid-crystalline semiconducting polymers with high charge-carrier mobility

IAIN MCCULLOCH[1]*, MARTIN HEENEY[1], CLARE BAILEY[1], KRISTIJONAS GENEVICIUS[1], IAIN MACDONALD[1], MAXIM SHKUNOV[1], DAVID SPARROWE[1], STEVE TIERNEY[1], ROBERT WAGNER[1], WEIMIN ZHANG[1], MICHAEL L. CHABINYC[2], R. JOSEPH KLINE[3], MICHAEL D. MCGEHEE[3] AND MICHAEL F. TONEY[4]

[1]Merck Chemicals, Chilworth Science Park, Southampton S016 7QD, UK
[2]Palo Alto Research Center, Palo Alto, California 94304, USA
[3]Department of Materials Science and Engineering, Stanford University, California 94305, USA
[4]Stanford Synchrotron Radiation Laboratory, Menlo Park, California 94025, USA
*e-mail: iain.mcculloch@merckchem.co.uk

Published online: 19 March 2006; doi:10.1038/nmat1612

Organic semiconductors that can be fabricated by simple processing techniques and possess excellent electrical performance, are key requirements in the progress of organic electronics. Both high semiconductor charge-carrier mobility, optimized through understanding and control of the semiconductor microstructure, and stability of the semiconductor to ambient electrochemical oxidative processes are required. We report on new semiconducting liquid-crystalline thieno[3,2-*b*]thiophene polymers, the enhancement in charge-carrier mobility achieved through highly organized morphology from processing in the mesophase, and the effects of exposure to both ambient and low-humidity air on the performance of transistor devices. Relatively large crystalline domain sizes on the length scale of lithographically accessible channel lengths (~200 nm) were exhibited in thin films, thus offering the potential for fabrication of single-crystal polymer transistors. Good transistor stability under static storage and operation in a low-humidity air environment was demonstrated, with charge-carrier field-effect mobilities of 0.2–0.6 $cm^2\ V^{-1}\ s^{-1}$ achieved under nitrogen.

The search for materials to replace vacuum-deposited amorphous silicon (a-Si) as the active semiconductor in thin-film transistor (TFT) backplanes has involved intensive effort[1–3]. Significant progress has been made in the performance of transistors based on both single-crystalline[4,5] and thin-film vacuum-deposited organic semiconductors[6]. There are no efficient patterning technologies for vacuum-deposited organic materials, so additive, solution-based deposition processes offer attractive advantages. Although significant progress has been made to improve the performance of solution-deposited small molecules[7], polymers offer significant advantages in terms of solution rheology and mechanical properties. Semiconducting polymers, however, currently have lower performance than a-Si, limiting their application. Previous work has shown that conjugated main-chain thiophene polymers, in particular regioregular poly(3-hexylthiophene) (P3HT), exhibit a high charge-carrier mobility when pendant alkyl groups are attached in a regular head-to-tail arrangement[8,9]. This regioregularity promotes organization of the polymer backbone, creating a two-dimensional sheet-like lamella, which can be oriented with the thiophene ring plane orthogonal to the plane of the substrate by appropriate surface treatment[3,10]. Introducing unsubstituted thiophene units along the backbone and eliminating the presence of regioisomers in the polymer backbone were shown to retain this high charge-carrier mobility and to increase the ionization potential (IP) due to increased rotational freedom along the backbone[11,12]. In comparison to P3HT, this increase in IP imparts some improvement in oxidative stability. Self-assembly and crystallization were facilitated by the larger local free-volume between adjacent alkyl chains. The crystallite domain size that can be achieved by these materials, even after annealing within a liquid-crystal mesophase, is still small, 10–15 nm wide[13], and the maximum field-effect mobility is ~0.1–0.2 $cm^2\ V^{-1}\ s^{-1}$. As intermolecular charge hopping across grain boundaries, or through disordered domains, is not as efficient as within ordered domains[14], increasing the grain size is a promising approach to increase charge-carrier mobility.

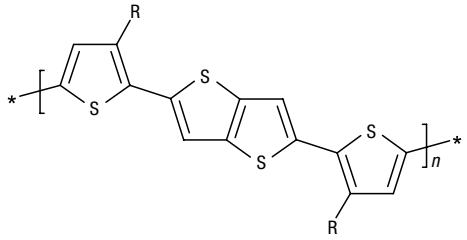

Figure 1 Chemical structure of poly(2,5-bis(3-alkylthiophen-2-yl) thieno[3,2-*b*]thiophene). $R = C_{10}H_{21}$, $C_{12}H_{25}$, $C_{14}H_{29}$.

Here we report a semiconducting polythiophene that is designed to assemble into large crystalline domains on crystallization from a liquid-crystal phase, and to possess an extended, planar π electron system that allows close intermolecular π–π distances, which facilitate high charge-carrier mobility. In addition, rather than increase the IP by sterically twisting the repeat units in the backbone, which intuitively should reduce the crystalline perfection, we incorporate a linear conjugated comonomer, thieno[3,2-*b*]thiophene. The delocalization of electrons from this fused aromatic unit into the backbone is less favourable than from a single thiophene ring, due to the larger resonance stabilization energy of the fused ring over the single thiophene ring. This reduced delocalization along the backbone results in a lowering of the polymer highest occupied molecular orbital level. Furthermore, the rotational invariance of the linearly symmetrical thieno[3,2-*b*]thiophene in the backbone facilitates the adoption of the low-energy backbone conformation, promoting formation of highly ordered crystalline domains.

The thieno[3,2-*b*]thiophene units were incorporated regiospecifically at the 2,5 position into the polymer backbone by a 1:1 co polymerization with a 4,4′-bialkythiophene comonomer, affording a series of poly(2,5-bis(3-alkylthiophen-2-yl)thieno[3,2-*b*]thiophenes) (PBTTT); Fig. 1. This synthetic preparation uses two symmetrical monomers, thus avoiding the regioirregularities that can occur during the polymerization of asymmetric monomers[15]. Tail-to-tail regiopositioning of the alkyl chains on the bithiophene monomer helps promote self-organization, while minimizing any steric interactions between the neighbouring alkyl groups, thus preserving backbone planarity.

The IP of the polymer series is about 5.10 eV (Table 1), which is approximately 0.3 eV greater than that of regioregular P3HT measured under identical conditions. Previously, the incorporation of a 2,2′-bithiophene unit into an alkyl thiophene backbone (poly[5,5′-bis(3-alkyl- 2-thienyl)-2,2′-bithiophene]; PQT) resulted in an increase in IP of approximately 0.1 eV (ref. 11), in comparison to that of P3HT, most probably as a result of the increased flexibility of the backbone reducing π–π overlap. In the present case, we suggest that the higher IP arises mainly from the reduced delocalization from the thienothiophene aromatic ring in comparison with thiophene, along with reduced electron donation from the fewer alkyl groups on the backbone than P3HT. The hypsochromic absorption maxima shift of about 20 nm (compared with P3HT) is also consistent with the increase in IP.

The thermal transitions of the polymers were investigated by differential scanning calorimetry (Table 1 and Supplementary Information). All three polymers exhibit at least two discrete endotherms on heating, and two exotherms on cooling. Both the C10 and C12 polymers show evidence of polymorphic behaviour, with an additional possible melting endotherm apparent on further heating just above the main melt endotherm. The highest temperature transitions were, in all cases, reversible on temperature cycling, and the cooling exotherm from the isotropic phase was relatively independent of the cooling rate. These factors are consistent with an isotropic liquid-crystal transition. The relatively high enthalpies (10−13 J g^{-1}) of this cooling transition, shown in Table 1, in comparison with similar nematic extended hairy rod conjugated mainchain polymers[13,16,17], suggests that the mesophase is not nematic. Increasing the alkyl chain length increased the mesophase temperature range, primarily by lowering the melting and crystallization temperatures ($T1\uparrow$ and $T1\downarrow$ in Table 1). The calorimetry data suggested that the microstructure of the materials should be strongly affected by thermal annealing. We therefore applied a combination of synchrotron X-ray scattering and atomic force microscopy (AFM) to examine thin films of PBTTT. These results show that the films contain crystalline domains that can be controlled using thermal annealing.

AFM images, shown in Fig. 2, illustrate that annealing thin films of C12 polymer above the liquid-crystal isotherm changes the morphology from a nodule-like structure with some fibrils to an oriented polycrystalline structure with 200-nm-diameter grains. The nodule-like structure of the as-spun film is typical of that observed for high molecular weight (MW) conjugated polymer films, whereas the large polycrystalline grains of the annealed film are unlike anything previously reported for solution-cast high-MW conjugated polymer films[18–21], and are comparable to polycrystalline films of some vacuum-deposited molecular organic films. On the basis of the molecular weight of the polymer, these lateral length-scales correspond to at least three polymer chains incorporated lengthwise into the largest crystalline domains. This morphology contrasts with that of similar systems, where domains have been reported to be only one polymer chain wide, for example, films of low-MW P3HT films with small rod-like crystals[18].

Detailed information about the crystalline domains observed in the AFM images was obtained using synchrotron X-ray scattering.

Table 1 Polymer properties. $T1\uparrow$ **and** $T2\uparrow$ **correspond to the low- and high-temperature endotherms on heating (at 10 °C min^{-1}) respectively, and** $T2\downarrow$ **and** $T1\downarrow$ **correspond to the high- and low- temperature exotherms on cooling (10 °C min^{-1}) respectively. IP was measured by an ambient ultraviolet photoelectron spectroscopy (UPS) technique.**

Sidechain	Mn/Mw	λ_{max} (nm)	IP (eV)	$T1\uparrow$ (°C)	$T2\uparrow$ (°C)	$T2\downarrow$ (°C)	$T1\downarrow$ (°C)	Cooling enthalpy $T2\downarrow$ (J g^{-1})	Cooling enthalpy $T1\downarrow$ (J g^{-1})	$\mu_{max\ sat}$ (N_2) (cm^2 V^{-1} s^{-1})	$\mu_{max\ lin}$ (N_2) (cm^2 V^{-1} s^{-1})	ON/OFF ratio (N_2)
C10	28,500/51,300			171	251	237	142	13.1	18.5	0.30	0.22	10^6
C12	29,600/54,000	547	5.1	143	244	233	115	10.1	20.5	0.30	0.11	10^6
C14	33,000/59,600			141	248	233	102	11.3	26.5	0.63	0.39	$>10^7$
										0.72*	0.20*	$>10^{6*}$

* Different device geometry ($W = 2{,}000$ μm, $L = 5$ μm) and dielectric thickness (200 nm).

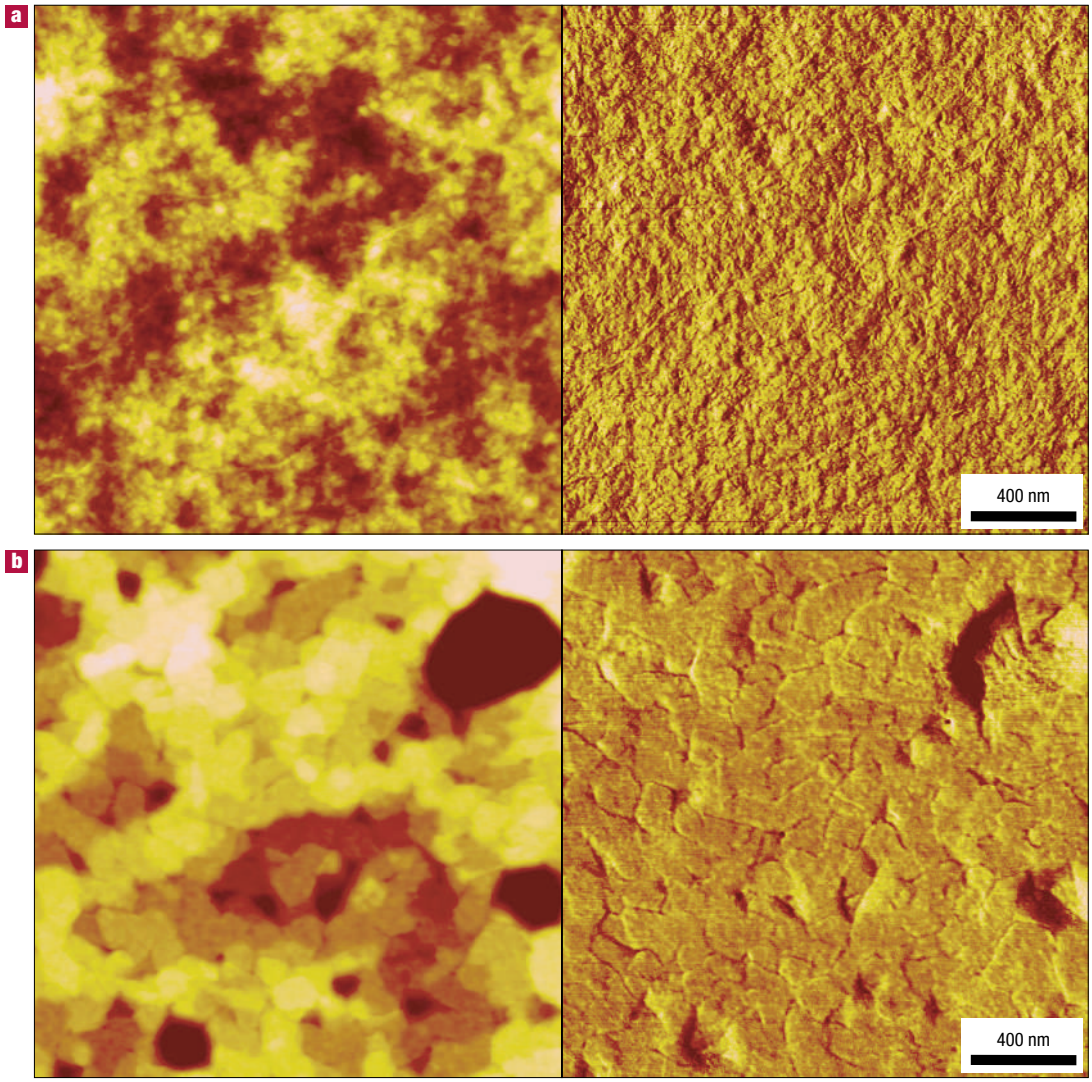

Figure 2 AFM images of polymer C12 (annealed at 180 °C). a, Before and **b**, after annealing above the liquid-crystal isotherm. The left images show the topography and the right images show the phase image. The dark spots in the topography of the annealed film are voids where the film partially dewetted during annealing.

Thin films of samples annealed at 100 °C, below any of the observed phase transitions, and at 180 °C, near one of the endotherms, both show peaks with spacings characteristic of a lamellar structure. The out-of-plane scattering for the films (Fig. 3a) shows a progression of peaks at a *d*-spacing of 19.6 Å. We have assigned this set of peaks as the *a*-axis (*h*00), the lamellar spacing. The distance is consistent with structural models, where the sidechains of the polymer are interdigitated or closely packed and tilted out of the molecular plane. The intensity of the peaks increases dramatically with annealing, and peaks up to the fifth order appear in films annealed at 180 °C. The X-ray scattering shown in Fig. 3a only probes crystallites that are highly oriented relative to the substrate, in this case those with planes parallel to the substrate. Thus, the change in intensity on annealing is probably due to a combination of the reorientation of molecules during heating and the growth of the size of existing crystalline regions, and is consistent with the large domains observed in the AFM images.

The in-plane structure was studied using grazing incidence X-ray scattering, which probes for crystalline planes oriented perpendicular to the surface (Fig. 3b). Both the 100 °C annealed sample and 180 °C sample show (0*k*0) peaks consistent with π-stacking (3.72 Å) without any evidence of (*h*00) spacings. This π-stacking distance is comparable to values reported for P3HT and PQT-12. The other peaks in the scattering pattern can be indexed as (00*l*) reflections based on an orthorhombic cell with the *c* axis equal to the length of the repeat unit (~13.3 Å). The high degree of orientation of the crystalline domains in these films is advantageous for charge transport, assuming that the region nearest the gate dielectric also has a structure similar to that of the bulk film.

The charge-carrier mobilities, μ, of these polymers are high, with values of 0.2–0.6 $cm^2\ V^{-1}\ s^{-1}$ obtained on annealed devices in a nitrogen atmosphere (Table 1), and up to 0.7 $cm^2\ V^{-1}\ s^{-1}$ for a 5 μm channel length device. Current–voltage characteristics for the C14-based TFTs with $\mu = 0.6$ and 0.7 $cm^2\ V^{-1}\ s^{-1}$ are shown in Fig. 4. Although the highest mobility was achieved for the C14 polymer, we believe that the mobility is also dependent on the device fabrication conditions, which may have been most favourable for the C14 analogue. Some variation in the onset voltage of the TFTs under different conditions was observed. Under nitrogen, the onset voltage derived from the transfer curves

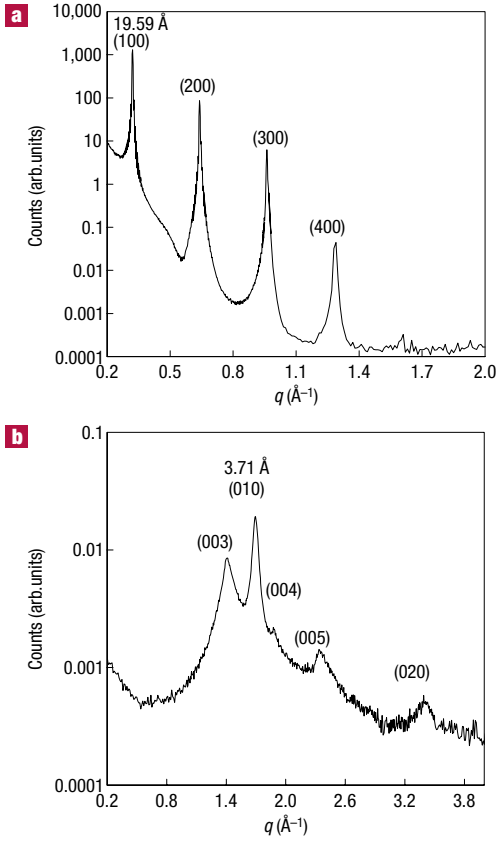

Figure 3 X-ray scattering pattern of polymer C12 (annealed at 180 °C). **a**, Out-of-plane and **b**, in-plane X-ray scattering. The crystallographic assignments of the peaks are labelled.

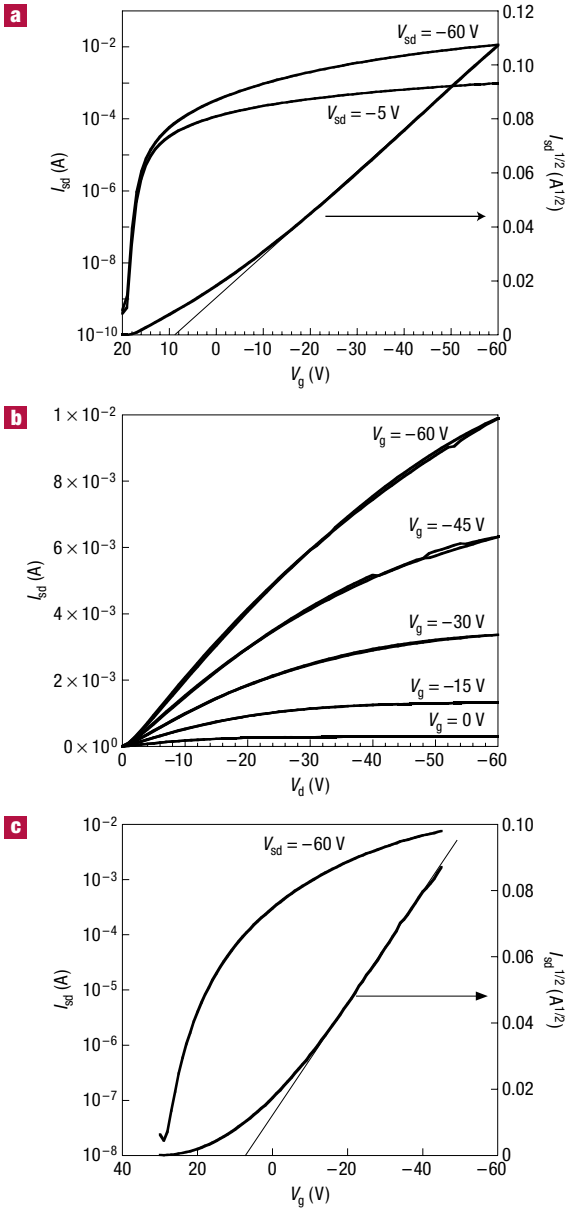

Figure 4 Field-effect transistor device characteristics in N_2 atmosphere with polymer C14 semiconductor. **a**, Transfer and **b**, output characteristics of a device with $W = 10{,}000$ μm and $L = 20$ μm, exhibiting a charge-carrier mobility of 0.6 $cm^2\ V^{-1}\ s^{-1}$; **c**, transfer characteristics of a device with $W = 2{,}000$ μm and $L = 5$ μm, exhibiting a charge-carrier mobility of 0.72 $cm^2\ V^{-1}\ s^{-1}$. V_{sd} is the source–drain voltage.

(Fig. 4a,c) is ∼+20 V to +30 V, whereas in ambient conditions (Fig. 5a) it is ∼+10 V, and in dry air (Fig. 5b) it is ∼−5 V. We do not currently fully understand the origin of this behaviour, although it appears to be related, in part, to the environment, but it is possible that there are contributions from the thermal processing history and the dielectric interface.

The mobility values for the PBTTT series are about one order of magnitude higher than benchmark comparisons of P3HT, also prepared and measured in our laboratories (see the Supplementary Information), and also larger than those of an analogous polymer synthesized in our laboratory[22] that incorporates an isomeric fused thienothiophene where the sulphur atoms are in a *syn* position. The performance of semiconducting polymers has generally lagged behind that of molecular semiconductors; these solution-processed polymers are comparable to most polycrystalline vapour-deposited films[1]. Importantly, the field-effect mobility of these materials is equivalent to that of a-Si TFTs used in commercial display backplanes.

The improvement in mobility is due to the improved control of crystallization. The polymers have been annealed in their liquid-crystalline phase, and subsequently allowed to crystallize on cooling. The X-ray and AFM data show that these films have grains that are as large as those observed for many molecular materials, and by this fact alone, we would anticipate a higher field-effect mobility than for materials with smaller grains (P3HT and PQT-12). Increased grain size is not necessarily connected to improvements in field-effect mobility, as transport across grain boundaries can limit the performance of TFTs (ref. 1). In these materials, organized assembly and orientation of the chains is facilitated in the liquid-crystalline phase, and this will be maintained on crystallization. It is expected that the regions between the discrete crystalline domains will have a more-organized morphology than a typical amorphous region that is commonly observed on crystallization from an isotropic melt. The specific volume difference between crystalline and liquid-crystalline phases is typically not as large as between crystalline and amorphous phases. On crystallization from the LC phase, the formation of crystallites would not be expected to create disorganized domains of high free-volume close to the crystallite

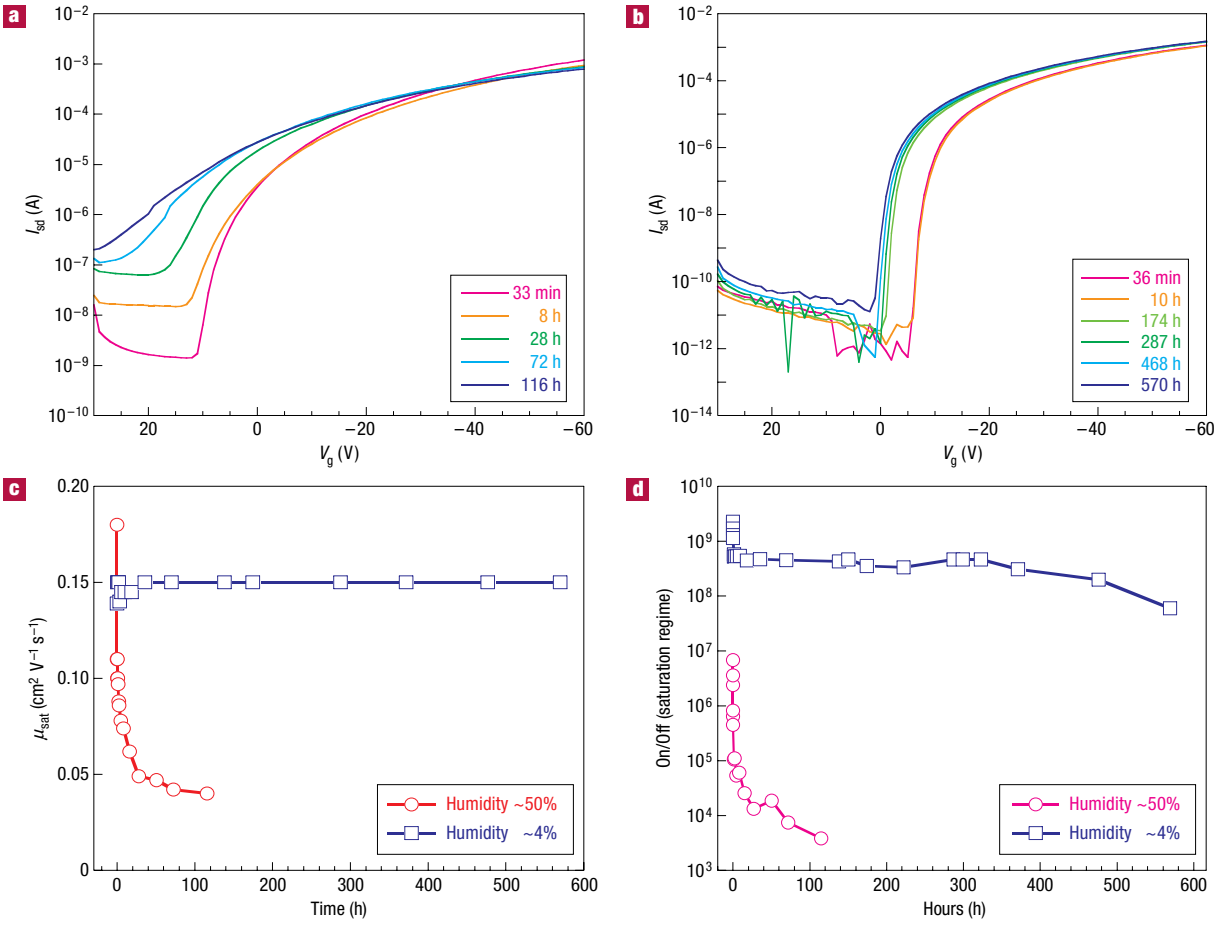

Figure 5 Stability of FET devices. Transfer characteristics for polymer C12 shown on prolonged exposure to **a**, ambient air and **b**, low humidity air. Change in **c**, mobility and **d**, ON/OFF ratio with time in both ambient and low-humidity air.

surfaces. It has been suggested that transport in semicrystalline polymers can be understood as percolation of carriers through a network of crystalline domains connected by amorphous regions; if the regions between the crystalline domains are more ordered, we expect that transport should be easier due to an improvement in connectivity of the network, and that charge trapping within these regions will be lower[14,23]. Thus, the improvement realized here is probably due to an overall improvement in the ordering and orientation of the films in both crystalline domains and within the more disordered regions between them.

In addition to high carrier mobility, these materials are also relatively stable. Current–voltage measurements carried out in ambient air (humidity level ~50%) show good electrical performance during the first few days (see Fig. 5a–d). After five days in ambient conditions, the mobility decreased by a factor of two, and the ON/OFF ratio was reduced by two orders of magnitude. In comparison, the electrical performance of the polymers on exposure to low-humidity (~4%) air shows good stability, with almost unchanged mobility, only a small positive threshold voltage shift, and a slight decrease of ON/OFF ratio. Furthermore, devices in a low-humidity environment were measured for more than 20 days and showed good performance: the field-effect mobility of the transistor in the saturation regime $\mu_{\mathrm{FET\ sat}} = 0.15\ \mathrm{cm^2\ V^{-1}\ s^{-1}}$, ON/OFF $\approx 8 \times 10^7$ and the onset voltage $V_t \approx 0$ V. These trends are in good agreement with measurements carried out with P3HT, which also show slower degradation at lower humidity levels[24]. The increased IP of the polymers, in comparison to P3HT, is reflected in the improved environmental stability. Electrochemical oxidation in ambient air[25] is less favourable, and hence simple doping, which manifests as both a shift to more-positive threshold voltages and higher OFF currents, will be reduced, although this behaviour can still be observed in the transfer characteristics (Fig. 5a) of transistors exposed to ambient air and humidity. These environmental stability results suggest that the routine encapsulation schemes used in practical TFT device structure fabrication will be adequate to preserve performance.

Our results illustrate that for the first time, mobilities equivalent to amorphous silicon can be achieved with printable semiconducting polymers. These materials have unusual morphological properties relative to other rigid-rod polymers. Additionally, the relatively large size of the crystalline domains in these materials are well within reach of the nanoscale features that can be fabricated using many lithographic and printing techniques[26,27], suggesting that these materials can be used to answer important questions about electrical transport within single-crystalline domains in semiconducting polymers.

METHODS

The polymers were prepared by a Stille copolymerization between 2,5-bis(trimethylstannyl)thieno[3,2-*b*]thiophene and the appropriate

5,5′-dibromo- 4,4′-dialkyl-[2,2′]-bithiophene in analogy to a previously reported procedure (see Supplementary Information for full experimental details)[28]. AFM images were obtained using a multimode AFM (Veeco) in tapping mode in air using Tap-150 silicon probes (Veeco). Fresh tips were used with each sample, to avoid image convolution due to tip contamination. AFM samples were identical to those used in X-ray analysis. Measurements of X-ray scattering were carried out at the Stanford Synchrotron Radiation Laboratory on beam line 7-2. The incident energy was 8 keV. The samples were kept under a helium atmosphere during irradiation to minimize damage to the films from the beam. For grazing incidence X-ray scattering (GIXS), the films were illuminated at a constant incidence angle of 0.2°, and the X-ray beam penetrated the entire thickness of the sample (~100 nm) and a portion (<10 nm) of the silicon substrate. The GIXS data were corrected for the area of illumination based on the slits used for the incident and exiting beam and sample size[29]. Ionizaton potentials were determined by an ambient photoelectron spectroscopy method with a Riken-Keiki AC-2 spectrometer[30]. The absorption maxima were collected by a Perkin Elmer Lambda 9 UV-VIS spectrophotometer. Thermal properties of the polymers were obtained with a TA Q1000 differential scanning calorimeter. Heating and cooling rates were 10 °C min^{-1}, where heating data for the second scan were used. Organic FETs were fabricated under dry nitrogen, on highly-doped silicon substrates with a 230-nm-thick thermally grown SiO_2 insulating layer, which was used as a common gate electrode. Transistor source–drain gold electrodes were deposited by photolithography. Before organic semiconductor deposition, the substrates were treated with silylating agent octyltrichlorosilane (OTS) by immersing them in 10-mM solutions in toluene for 15 min at 60 °C. Organic semiconductor layers were deposited by spin-coating from ~0.5−1 wt% solutions in warm 1,2-dichlorobenzene. Typical film thickness was 30–60 nm (measured by a KLA Tencor Alpha-Step 500 profilometer). After spin-coating, transistor samples were then annealed at the high-temperature edge of the melting transition (120−160 °C) for 10–15 min. For all of our measurements, we used FET channel lengths (L) of 5−20 μm and channel widths (W) of 2,000−10,000 μm. FET characterization was carried out using an Agilent 4155C semiconductor parameter analyser. Field-effect mobilities were extracted in the linear regime from the slope of the source–drain current in the linear regime (I_{sd}^{lin}) versus the gate voltage (V_g) I_{sd}^{lin} versus V_g plots, and in the saturation regime were calculated from the linear fit of $\sqrt{I_{sd}^{sat}}$ versus V_g (where I_{sd}^{sat} is the source–drain current in the saturation regime). The turn-on voltage (V_0) was determined as the onset of the source–drain current from the log-lin I–V plot. The air stability of the FETs was determined by exposing devices made and annealed under nitrogen to air with a controlled humidity level, and measuring the device I–V characteristics over an extended time period.

Received 3 October 2005; accepted 13 February 2006; published 19 March 2006.

References

1. Katz, H. E. Recent advances in semiconductor performance and printing processes for organic transistor-based electronics. *Chem. Mater.* **16,** 4748–4756 (2004).
2. Chabinyc, M. L. & Salleo, A. Materials requirements and fabrication of active matrix arrays of organic thin film transistors for displays. *Chem. Mater.* **16,** 4509–4521 (2004).
3. Sirringhaus, H. *et al.* Two-dimensional charge transport in self-organized, high-mobility conjugated polymers. *Nature* **401,** 685–688 (1999).
4. Jurchescu, O. D., Baas, J. & Palstra, T. T. M. Effect of impurities on the mobility of single crystal pentacene. *Appl. Phys. Lett.* **84,** 3061–3063 (2004).
5. Podzorov, V., Sysoev, S. E., Loginova, E., Pudalov, V. M. & Gershenson, M. E. Single-crystal organic field effect transistors with the hole mobility. Approx. 8 cm^2/Vs. *Appl. Phys. Lett.* **83,** 3504–3505 (2003).
6. Baude, P. F. *et al.* Pentacene-based radio-frequency identification circuitry. *Appl. Phys. Lett.* **82,** 3964–3966 (2003).
7. Payne, M. M., Parkin, S. R., Anthony, J. E., Kuo, C. C. & Jackson, T. N. Organic field-effect transistors from solution-deposited functionalized acenes with mobilities as high as 1 $cm^2/V \cdot s$. *J. Am. Chem. Soc.* **127,** 4986–4987 (2005).
8. Sirringhaus, H., Tessler, N. & Friend, R. H. Integrated optoelectronic devices based on conjugated polymers. *Science* **280,** 1741–1744 (1998).
9. Bao, Z., Dobabalapur, A. & Lovinger, A. J. Soluble and processable regioregular poly(3-hexylthiophene) for thin film field-effect transistor applications with high mobility. *Appl. Phys. Lett.* **69,** 4108–4110 (1996).
10. Prosa, T. J., Wimokur, M. J., Moulton, J., Smith, P. & Heeger, A. J. X-ray structural studies of poly(3-alkylthiophenes): An example of an inverse comb. *Macromolecules* **25,** 4364–4372 (1992).
11. Ong, B. S., Wu, Y., Liu, P. & Gardner, S. High-performance semiconducting polythiophenes for organic thin-film transistors. *J. Am. Chem. Soc.* **126,** 3378–3379 (2004).
12. McCulloch, I. *et al.* Influence of molecular design on field-effect transistor characteristics of terthiophene polymers. *Chem. Mater.* **17,** 1381–1385 (2005).
13. Zhao, N. *et al.* Microscopic studies on liquid crystal poly(3, 3‴-dialkylquaterthiophene) semiconductor. *Macromolecules* **37,** 8307–8312 (2004).
14. Street, R. A., Northrup, J. E. & Salleo, A. Transport in polycrystalline polymer thin-film transistors. *Phys. Rev. B* **71,** 165202 (2005).
15. McCullough, R. The chemistry of conducting polythiophenes. *Adv. Mater.* **10,** 93–116 (1998).
16. Brennan, D. J. *et al.* Recent advances in the synthesis of polyfluorenes as organic semiconductors. *Mater. Res. Soc. Symp. Proc.* **814,** 1–12 (2004).
17. Heeney, M. *et al.* Alkylidene fluorene liquid crystalline semiconducting polymers for organic field effect transistor devices. *Macromolecules* **37,** 5250–5256 (2004).
18. Kline, J. R., McGehee, M. D., Kadnikova, E. N., Liu, J. & Frechet, J. M. J. Controlling the field-effect mobility of regioregular polythiophene by changing the molecular weight. *Adv. Mater.* **15,** 1519–1522 (2003).
19. Babel, A. & Jenekhe, S. A. Field-effect mobility of charge carriers in blends of regioregular poly(3-alkylthiophene)s. *J. Phys. Chem. B* **107,** 1749–1754 (2003).
20. Yang, H. C. *et al.* Effect of mesoscale crystalline structure on the field-effect mobility of regioregular poly(3-hexylthiophene) in thin-film transistors. *Adv. Funct. Mater.* **15,** 671–676 (2005).
21. Kline, R. J. *et al.* Dependence of regioregular poly(3-hexylthiophene) film morphology and field-effect mobility on molecular weight. *Macromolecules* **38,** 3312–3319 (2005).
22. Heeney, M. *et al.* Stable polythiophene semiconductors incorporating thieno[2,3-b]thiophene. *J. Am. Chem. Soc.* **127,** 1078–1079 (2005).
23. Salleo, A. *et al.* Intrinsic hole mobility and trapping in a regioregular poly(thiophene). *Phys. Rev. B* **70,** 115311 (2004).
24. Meijer, E. J. *et al.* Dopant density determination in disordered organic field-effect transistors. *J. Appl. Phys.* **93,** 4831–4835 (2003).
25. Leeuw, D. M. d., Simenon, M. M. J., Brown, A. R. & Einerhand, R. E. F. Stability of n-type doped conducting polymers and consequences for polymeric microelectronic devices. *Synth. Met.* **87,** 53–59 (1997).
26. Xia, Y., Rogers, J. A., Paul, K. E. & Whitesides, G. M. Unconventional methods for fabricating and patterning nanostructures. *Chem. Rev.* **99,** 1823–1848 (1999).
27. Sele, C. W., von Werne, T., Friend, R. H. & Sirringhaus, H. Lithography-free, self-aligned inkjet printing with sub-hundred nanometer resolution. *Adv. Mater.* **17,** 997–1001 (2005).
28. Tierney, S., Heeney, M. & McCulloch, I. Microwave-assisted synthesis of polythiophenes via the stille coupling. *Synth. Met.* **148,** 195–198 (2005).
29. Toney, M. F. & Wiesler, D. G. Instrumental effects on measurements of surface x-ray diffraction rods: Resolution function and active sample area. *Acta Crystallogr. A* **49,** 624–642 (1993).
30. Sano, T., Hamada, Y. & Shibata, K. Energy-band schemes of highly stable organic electroluminescent devices. *IEEE J. Sel. Top. Quantum Electron.* **4,** 34–39 (1998).

Acknowledgements

Portions of this research were carried out at the Stanford Synchrotron Radiation Laboratory, a user facility operated by Stanford University on behalf of the US Department of Energy, Office of Basic Energy Sciences.
Correspondence and requests for materials should be addressed to I.M.
Supplementary Information accompanies this paper on www.nature.com/naturematerials.

Competing financial interests

The authors declare that they have no competing financial interests.